

Data acquisition and reduction

Contents

3.1	Introduction	37
3.2	Data acquisition	38
3.2.1	DANDICAM	38
3.2.2	Photometric observations	39
3.2.3	The 1.9-m telescope and long slit spectrograph	40
3.2.4	Spectroscopic observations	40
3.3	Reduction of the photometric images	41
3.3.1	Bias subtraction	42
3.3.2	Trim and OVERSCAN	42
3.3.3	Bad pixel mask and flat-field division	43
3.3.4	Photometric calibration with standard stars	45
3.3.5	Point-spread-function photometry	49
3.3.6	Matching source in V, R, I and R, I sets and correspondence with NIR sources	51
3.4	Spectroscopic reduction	53
3.4.1	Manual reduction	53
3.4.2	Automatic reduction	57

3.1 Introduction

In this chapter, a description is given of how the data used in this study were obtained and reduced. Three data sets were used in this study. The first was a set of photometric observations and the second and third sets were spectroscopic observations. The photometric and first spectroscopic sets were compiled from observations made during the first two weeks of February 2002 respectively. After the results from these two data sets and the results of the NIR study by de Villiers (2009) were evaluated, it was possible to compile a list of candidate objects for further spectroscopic observations as the third data set. This set was obtained by means of observations taken during the last week of February 2011.

3.2 Data acquisition

3.2.1 DANDICAM

The photometric data that were used in this dissertation were obtained with the DANDICAM camera, a description of which follows.

According to the DANDICAM page on the PLANET (Probing Lensing Anomalies NETwork) collaboration's website (<http://planet.iap.fr/dandicams.html>) DANDICAM is a copy of the ANDICAM (A Novel Double-Imaging CAMera) and both were commissioned in 1998 for use in the PLANET collaboration project. The "D" in DANDICAM was added due to the Dutch ownership of the equipment, i.e. **D**utch ANDICAM. The camera was designed to be able to observe simultaneously in the optical and NIR filters and search for exosolar planets by means of micro-lensing. Both cameras were built by the Ohio State University under direction of Dr. Darren Depoy. The cameras are identical in all

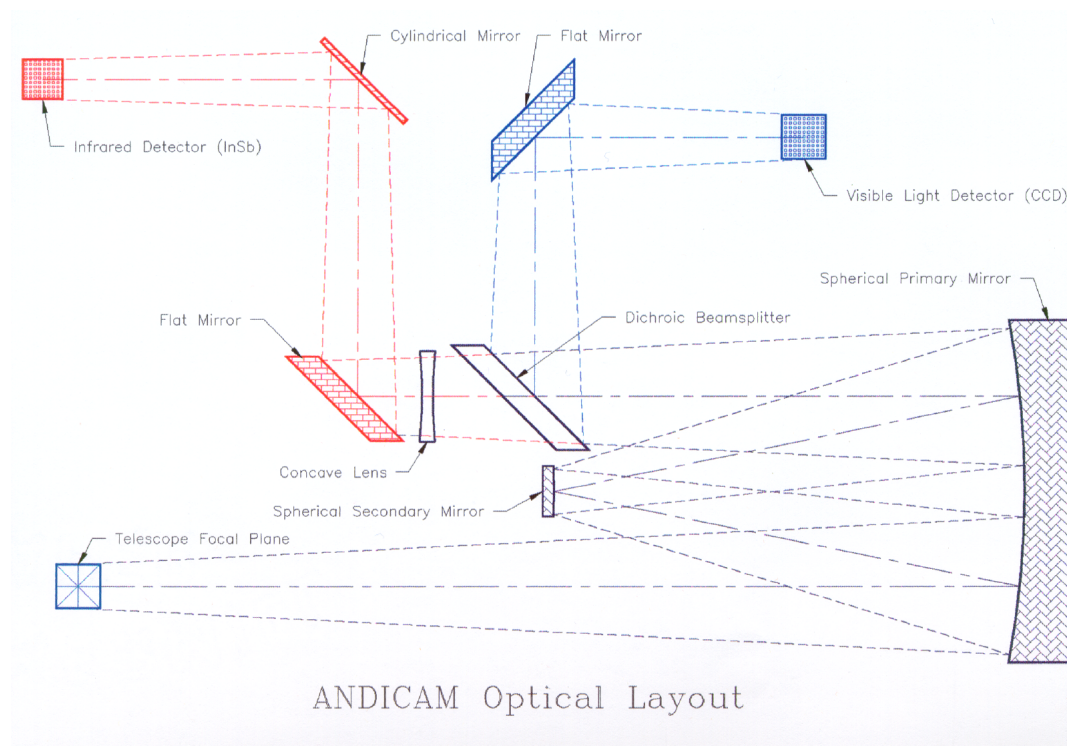


Figure 3.1: A layout of the optical systems for the DANDICAM and ANDICAM cameras as found on the DANDICAM webpage.

aspects except for the optical layout, as the 1-m telescope at CTIO in Chile has a focal length of $f/10$ and the 1-m telescope in Sutherland has a focal length of $f/15$. To keep the images on the same angular scale the optical layout for the one in Sutherland was changed slightly.

The two cameras were designed to perform very high precision optical and NIR photometry of a large field of view. The plate-scale of the optical CCD is $0.3''$ per pixel on an array of 2048×2048 pixels with a 15 micron pixel size. This CCD is a conjunction of two 1024×2048 CCDs. The NIR also

has a plate-scale of $0.3''$ per pixel with a resolution of 1024×1024 pixels and a pixel size of 27 micron. The CCDs were of very high quality at the time of construction giving a 20% throughput in the U filter and $>35\%$ throughput in the other filters. According to Bloom et al. (2004) ANDICAM has a Kron-Cousins filter-system, and with the knowledge that ANDICAM's and DANDICAM's optical systems are identical one can assume that DANDICAM has an identical optical filter system.

3.2.2 Photometric observations

As mentioned in chapter one, observations made in 2002 and used in this study were not obtained first hand by the author. These observations were initially for a study on the massive exciting star rather than the cluster of young stars, that was discovered by de Villiers (2009). The photometric set was part of observations of the southern high mass star forming regions RCW 34, NGC 2183, NGC 2626 and NGC 3576.

The photometric images were taken during the nights of 6, 7, 9 and 10 February 2002 on the 1.0-m (Elizabeth) telescope located at the SAAO in Sutherland, South Africa. The telescope's geographic location is S $32^\circ 22' 47.0''$, E $20^\circ 48' 36.3''$ at a height of 1798 m above mean sea level (AMSL). The telescope has a cassegrain focus of $f/16$ which gives a resolution of 12.94 arcsec/mm on an attached CCD. The FWHM for the seeing had a value ranging from 1.4 to 2.2 arcseconds during the week of observation. Observations of the high mass star forming region RCW 34 were obtained in the U, B, V, R and I colour filters. The field was centered on the methanol maser, as shown in Figs 1.3b and 1.5.

The exposure time for each observation was 600 seconds for each filter, with a few exceptions of 300 and 150 second exposures. To collect the maximum light on a CCD image from very dim objects the chip has to be exposed for as long as possible to incident light but not too long, as the image may become saturated. If a CCD is exposed for too long to a light source it can either become saturated by the light from the observed object or from the accumulation of cosmic rays which contaminate the image so that it is rendered useless. The total exposure time of each image that used for each filter is given in Table 3.1.

Exposure time	Seconds
t_U	960
t_B	3110
t_V	2850
t_R	2250
t_I	2250

Table 3.1: The total exposure times for various colour filters.

3.2.3 The 1.9-m telescope and long slit spectrograph

According to the Astronomical Society of Southern Africa's website (<http://assa.saa.ac.za/html/his-obs-radcliffe.html>) the 1.9-m telescope was built by Grub Parsons in 1938/9 for the Radcliffe observatory in Pretoria. Construction of the telescope was delayed due to the second world war and it only saw first light in 1948. In the 1960's relocation of the three main observatories in Pretoria, Cape Town and Johannesburg to Sutherland in the Karoo commenced due to light pollution in these cities. In 1974 the 1.9-m telescope was moved to Sutherland and has been operational since then, having undergone numerous upgrades.

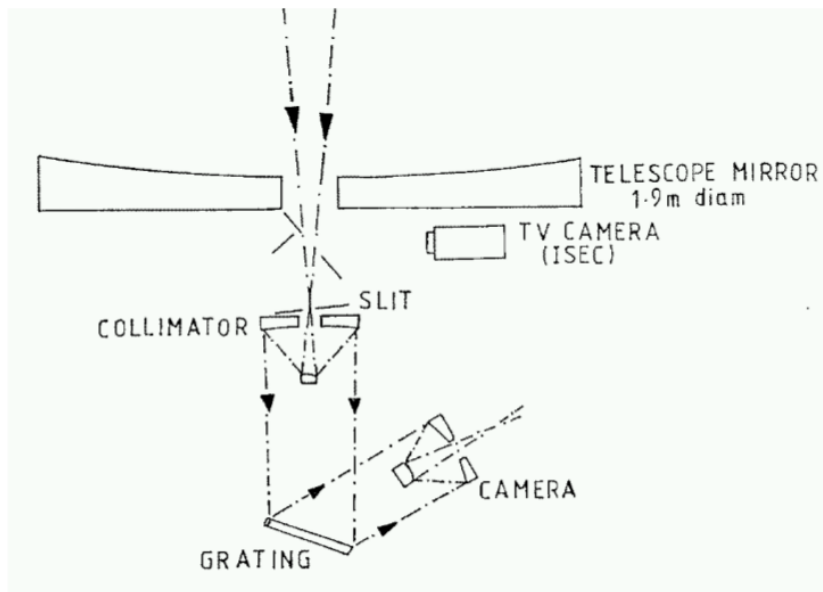


Figure 3.2: This image was taken from the manual for the 1.9-m telescope, found on the website for the SAAO (<http://www.saa.ac.za/>). When light moves into the 1.9-m telescope, it gets distributed onto a larger scale, depending on the slit width and the angle of the grating, making the absorption and emission lines which fall into the specific region of interest much more apparent.

The optical layout of the long-slit spectrograph is shown in Fig 3.2. The telescope has a 2-pier asymmetrical mounting from which it is only possible to do observations from the Eastern side of the pier. It has a Cassegrain focus of $f/18$, which is equivalent to a roughly 6 arc-sec/mm resolution.

The slit should be used to let in as much light as possible from the source, while cutting out light from other sources in the telescope's field of view. The slit width is in the range of a few hundred μ -meters. The telescope has two finder scopes but the long-slit spectrograph has an acquisition camera built into the optics, so that alignment with an object is done from the warm-room. The 1.9-m telescope and long slit spectrograph were used for all of the spectroscopic observations in this dissertation.

3.2.4 Spectroscopic observations

The first set of observations was collected by D.J. Van der Walt for the purpose of demonstrating the reduction of long slit spectra. The second set was obtained by the author by means of observations

based on optimised planning which included the results from the NIR study by de Villiers (2009) as well as the photometric and spectroscopic observations of the first two sets of 2002.

The spectroscopic observations of 2002 and 2011 were performed using the 1.9-m (Radcliffe) telescope at the SAAO near Sutherland, South Africa. The telescope is at the same elevation and closely situated to the location of the 1.0-m telescope used for the photometric observations at a geographic position of S 32° 22' 44.2", E 20° 48' 41.9", 1798m AMSL. The telescope has a Cassegrain focus of $f/18$ which gives a resolution of 6 arcsec/mm on an attached CCD.

The long slit spectrograph was used with grating number 6 in 2002 and grating number 7 in 2011. The resolution of grating 6 is 2 Å and for grating 7 it was 5 Å. Grating number 6 could not be used for the observations of 2011 because it was damaged. The slit width used in 2002 was 300 μm and 250 μm in 2011. The 2002 observations were conducted in the blue and red parts of the visible spectrum. The median wavelength is 4500 Å for the blue part and 5900 Å for the red part of the spectrum, each spanning a range of 2000 Å. Only one grating configuration was used for the observations of 2011. This included the red and blue part of the spectrum, centred at 5400 Å and spanning from 3700 Å to 7700 Å.

3.3 Reduction of the photometric images

Raw images captured on a CCD have to undergo a few reduction steps before they can be used for scientific measurements. An image taken with a CCD first has to be corrected for noise originating from the electronics. After this the image has to be corrected for thermal noise. Further corrections have to be made for dust in the observation equipment and irregularities in the optics. The images were reduced using version 2.14.1 of the IRAF (Image Reduction and Analysis Facility) software package. The reduction followed the steps outlined in "A user's guide to CCD reduction with IRAF" by Philip Masey, which is freely available on the NOAO website.

Three types of images are required to reduce the captured CCD images for analysis: BIAS, DARK and FLATFIELD images. The BIAS images are blank readouts received from the CCD by the computer system. These are used to correct the captured images for noise that occurs when the image is read from the CCD. When an image is read from the CCD after an exposure, the chip amplifiers and the analog-to-digital converters have an error on each pixel so that each time an image is read from the CCD it will not give the same value. To get a good statistical approximation of what number of electrons are added to a specific pixel upon readout, an averaged BIAS image is constructed from numerous blank readouts. For visual representations of how an image looks before and after BIAS subtraction, see the example in Martinez & Klotz (1997).

If the temperature of the silicon in a CCD is high enough, the valence electrons can fall into the potential well of a pixel. To correct an image for the contamination by thermal electrons a DARK image is used. This is an image taken with the CCD when the camera shutter is closed. A set of

DARK images is usually taken at the same exposure time as the images of the objects of which the photometric measurements are taken, and is used to construct an average DARK image. On each image there are a few rows and columns of pixels that are not exposed to incident light. This part of the CCD is called the OVERSCAN region. The OVERSCAN region serves the same purpose as the DARK images but giving a value for the contamination by thermal electrons for every image.

A **flatfield** image is a uniformly illuminated background image which is out of focus, usually an image of a blank screen or of the dusk sky which reveals the different responses of the pixels across the CCD. The **flatfield** is also used to correct for the effects caused by dust or other small non-uniformities in the optics. To reduce an image of an object from which measurements are taken, the average BIAS image is subtracted to remove the noise due to the amplifiers and analog-to-digital converter. After this the average DARK frame is subtracted from the image of the object to remove the noise caused by thermal electrons. Lastly, the image of the object from which measurements are taken is divided by the **flatfield** image to remove the non-uniformities caused by errors in the optics or dust in the optics.

The default format in which CCD images are saved onto a computer system is the FITS (**F**lexible **I**mage **T**ransport **S**ystem) format, which is one of the standard formats for storing astronomical data. A FITS file has a header at the beginning of the file which is a set of 80 character text strings containing the properties of the observation instrument and values of parameters used in the reduction process of the image. The rest of the file can contain 1D data values, a 2D image or a 3D data cube of data. The image data can either be stored in integer or floating point format. The file can also store non-image based Tables with multiple data formats.

3.3.1 Bias subtraction

The first step was to construct an average BIAS Image. The BIAS images are directly read out from the CCD, and have zero exposure time. The set was constructed before observations commenced. The final BIAS image was constructed by using the **zerocombine** task in IRAF. Each pixel in the new image was the median for the pixels at the same coordinate in the set of BIAS images. The BIAS Image was subtracted from each of the **flatfield** images and from the images of the object frames with the **ccdproc** task.

3.3.2 Trim and OVERSCAN

The next step was to determine how much had to be trimmed from the edges of the images to yield only useful parts of raw images for data extraction. The OVERSCAN region and the edges of the CCD do not contain data relevant to scientific measurements, so these parts of each image are trimmed off, leaving only the useful part of each image. There were no DARK images in the provided datasets so the contamination by thermal electrons was removed from each image by using its OVERSCAN region.

Generally the trim and OVERSCAN regions of a chosen CCD image are written into the header of the FITS files, but this was not the case for the DANDICAM images. Hence, manual inspection of the images was required. If one views a layout of a `flatfield` image such as shown in Fig 3.3a and 3.3b, the counts drop from the one CCD to the conjoined counterpart in a trace across one of the middle columns. This is the result of the different responses of the conjoined CCDs. For each CCD a different OVERSCAN region had to be used. Personal communication with Dr. John Menzies of the SAAO confirmed this and he made available an `IRAF` script which declared the OVERSCAN regions of each of the CCDs on DANDICAM. The given script was successfully applied to all the images, achieving OVERSCAN reduction for each region of the images from each CCD separately. The script is presented in appendix A.

The readout noise due to the amplifiers and the electron gain of the CCD were also not available. However the values for ANDICAM were used. The values are similar those of the MK-1 DANDICAM. The data used are given in Table 3.2.

Parameter	Value
Pixel size :	15 micron
Pixel scale :	3 arc secs/pixel
Field of view :	10 × 10 arc seconds
Gain :	3.6 electrons/DN
Readout :	11 electrons/pixel

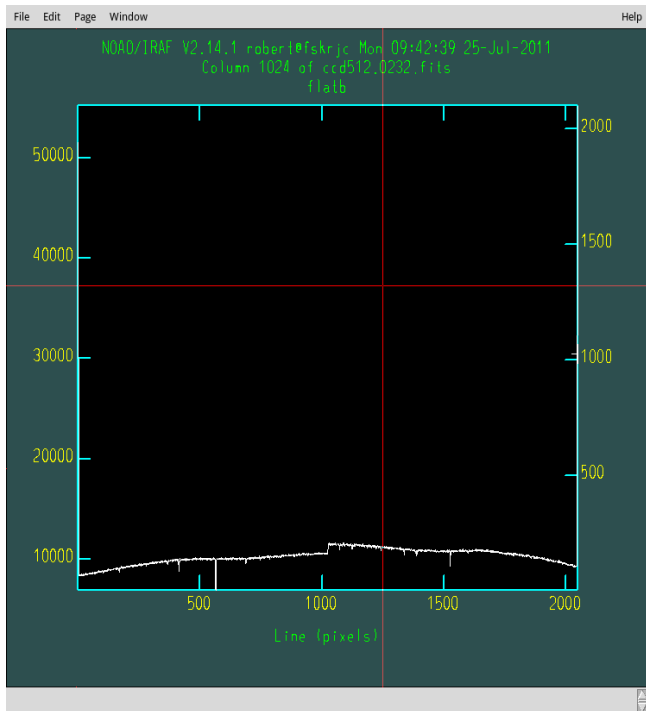
Table 3.2: The properties for the CCDs of ANDICAM and DANDICAM.

As shown in Fig 3.3c, near the edges of each image, pixel values increase to a very high value and then plummet to zero. This is the effect of the OVERSCAN region running up to the edge of the CCD. Close to the edge of the CCD the sensitivity becomes non-linear causing the read values to blow up. The images were trimmed in such a way that the maximum information could be used without contamination from the OVERSCAN region and the non-linear readouts.

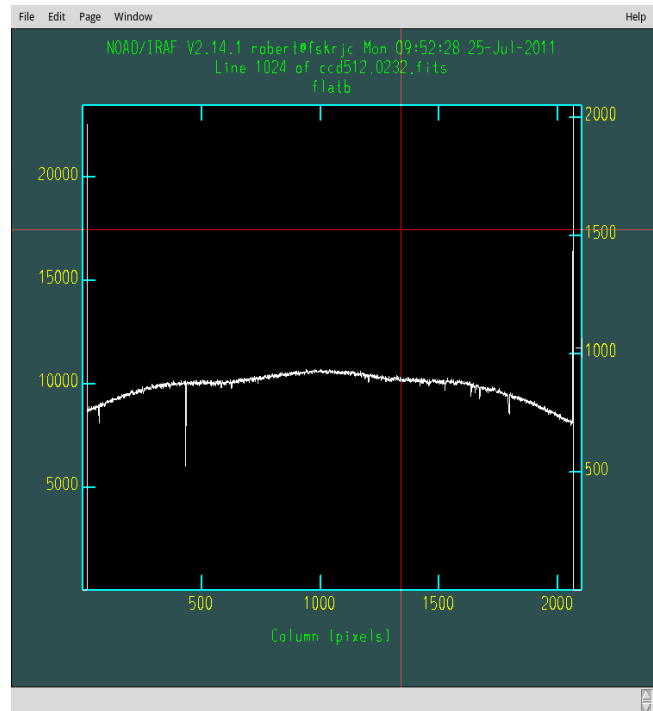
Vignetting was also noticed on the `flatfield` and object images. The vignetting differed slightly for each filter, and the usable area for the CCD images was selected from the `flatfield` image for each filter. The usable areas for each filter's images are listed in Table 3.3. The BIAS subtraction and trimming was done with the `noao.ccdred.ccdproc` task.

3.3.3 Bad pixel mask and flat-field division

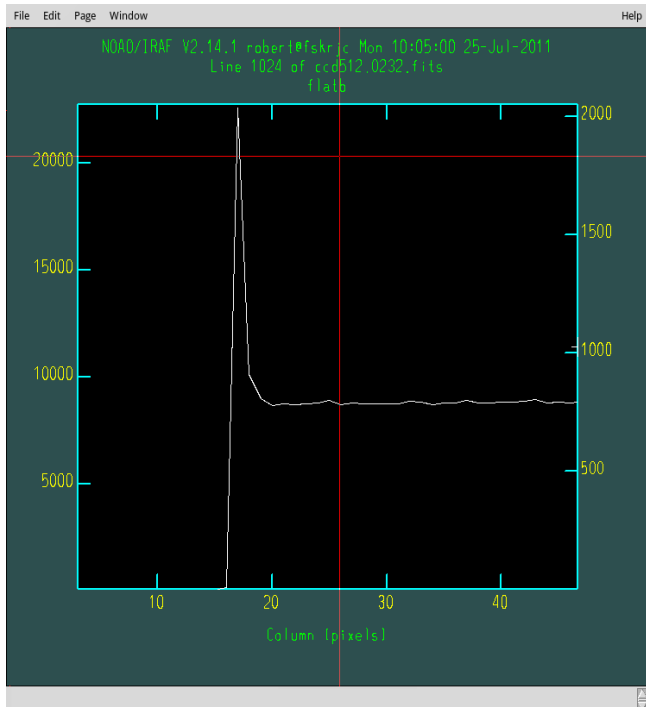
After the average BIAS image was subtracted from all of the images, treated for the OVERSCAN and trimmed, the images had to be corrected for irregularities caused by the optics and for variation in the pixel to pixel sensitivity. For photometry sky flats were sufficient for reduction, such that dome flats were not necessary.



(a) A plot through the middle line of one of the flat field images in the B filter.



(b) A plot through the middle column of one of the flat field images in the B filter.



(c) The edge of the raw B filter flat field image along the middle line plot.

Figure 3.3: Lines, columns and middle line plots through the *B* flatfield image.

Filter	x_{begin}	x_{end}	y_{begin}	y_{end}
U	150	1910	170	1910
B	120	1915	160	1930
V	150	1920	150	1920
R	125	1900	140	1880
I	120	1920	120	1920

Table 3.3: The usable region for each filter.

A useful tool that can be constructed from the **flatfield** images is a bad pixel mask. This is an overlay of a **FITS** image indicating pixels on the CCD which are not linear. Given a bad pixel mask, the reduction software interpolates values for the marked pixels from the surrounding unmarked pixels. The bad pixel mask can be constructed from **flatfield** images with high numbers of counts and low numbers of counts. The two images with the shortest exposure times were used as a set of "low count" **flatfield** images and the five with the longest exposure times were used as a set of "high count" exposures. The high count set was used to construct an averaged high count **flatfield** image with **flatcombine**. The same was done for the low count set. The high count image was divided by the low count image with the **imarith** task and a bad pixel mask was constructed with the procedure **ccdmask** from the divided image. The bad pixel mask was trimmed for each filter's images so that it matched the dimensions of the usable area of the filter images.

Flatfield images were taken on different occasions throughout the observation run. An average **flatfield** image was constructed for each filter with the **noao.ccdred.imred.flatcombine** task. The images of the objects were lastly processed again with **ccdproc**, this time with flatfielding and bad pixel correction.

3.3.4 Photometric calibration with standard stars

A standard photometric system is used so that any star has the same apparent magnitude when observed with any telescope, regardless of its location. Each telescope will measure a different instrumental magnitude for a star, so to calibrate the observed magnitudes of the star onto the standard system a set of standard stars is used to calculate the effects of atmospheric extinction, etc. Some of the main mechanisms in the atmosphere that affect incident star light are absorption by molecules, Rayleigh scattering by molecules or Mie scattering by small spherical particles. Rayleigh scattering causes incident light to scatter in any direction and the effect is proportional to $\lambda^{-4.1}$. Mie scattering is less random than Rayleigh scattering and causes a scattered photon to have the highest probability to propagate in the direction that it was travelling before it was scattered. The effects of Mie scattering are proportional to λ^{-1} . For more on the types of scattering that occur in the atmosphere see Chromey (2010).

To correctly calculate what the losses due to scattering and absorption in the atmosphere are, the angle of the star relative to the zenith is recorded. A unit of length to the zenith is dh and a unit of

length along the line of sight to the star that is observed is ds ; If one takes z to be the zenith angle and assume that the Earth's atmosphere is spherical, there exists a non-linear proportionality between z and the Earth's atmospheric thickness. The ratio of the fraction of the flux ($d\Phi'$) that is absorbed by the atmosphere in relation to the original flux (Φ') outside of the atmosphere is

$$\frac{d\Phi'}{\Phi'} = -\alpha(\lambda, h) ds = -\alpha(\lambda, h) ds = -\sec(z) \alpha(\lambda, h) dh, \quad (3.1)$$

where $\alpha(\lambda, h)$ is a measure of the absorption per unit length. The function $\tau(\lambda, H)$ is the optical thickness of the atmosphere at the zenith, which is calculated as

$$\tau(\lambda, H) = \int_0^H \alpha(h) dh. \quad (3.2)$$

If the flux [W/m^2] of light from a star is measured as $\Phi(\lambda)$ outside of the atmosphere then the flux at ground level $\Phi_A(\lambda)$ can be calculated as

$$\Phi_A(\lambda) = \Phi(\lambda) e^{-\int_0^H \sec(z(h)\alpha(h))dh} = \Phi(\lambda) e^{-\tau(\lambda, H)X}. \quad (3.3)$$

Where X is a parameter assigned to measure the thickness of the atmosphere, so that

$$X = \frac{s}{h} = \sec(z). \quad (3.4)$$

X is referred to as the **air mass**, and which is used to calculate the atmospheric extinction. A number of assumptions are made when the air mass is used to calculate the extinction caused by the atmosphere. The assumptions are that the path which is followed by the light is straight, the atmosphere is uniform and unchanging and the light in a filter is monochromatic. Now equation 3.3 is transformed to the magnitude scale

$$m_k^A = -2.5 \log \left[\frac{hc}{\lambda} \Phi_A(\lambda) \right] = -2.5 \log \left[\frac{hc}{\lambda} \Phi(\lambda) \right] + 2.5\tau(\lambda)X(z) \log(e) \quad (3.5)$$

$$m_\lambda^A = m_\lambda = 1.086\tau(\lambda)X, \quad (3.6)$$

where m_λ^A is the magnitude as measured from the observatory inside the atmosphere and m_λ is that which would be measured outside the atmosphere. The **monochromatic extinction coefficient** is now defined as $k(\lambda) = 1.086\tau(\lambda)$ so that equation 3.6 can be rewritten as:

$$m_\lambda^A(X) = m_\lambda + k(\lambda)X. \quad (3.7)$$

This linear transformation between the instrumental and apparent magnitude, using the air mass, is called **Bouguer's law**.

Standard stars are used for the calibration of stars observed from a ground based observatory. By using a standard star the extinction coefficient in equation 3.7 can be determined, making it possible to calculate the magnitude of the star on the standard photometric system and making it comparable with

results from other sites. Standard stars are not just used to calculate the effects of atmospheric extinction and to calibrate the apparent magnitudes on a standard system, but also to correct the colours of observed stars. This standard system makes it possible to get the same results for stars from different observation sites and make observations comparable to the data of other stars. Colours are a measure of the surface temperature of stars. The colour scale is calibrated to a zero point based on the colours of an A0 spectral type star with a surface temperature of 10 000 K. By using an iterative process and more than one standard star, the extinction coefficients can be determined to a high degree of accuracy.

A set of linear equations are used to calculate the relation between the magnitudes and the colours. One general set of transformation equations is the Landolt set, which is used to calculate the extinction for stars observed using Johnson-Cousins filters. The Landolt extinction equations have five orders of extinction coefficients: y_1, y_2, y_3, y_4 and y_5 (where y is a filter). A first order linear transformation of these equations is Bouguer's law, the set of calibration equations that were used are just higher order expansions of Bouguer's law Making the calibration of the magnitudes and colours much more precise. A set of linear transformations as given in equations 3.8-3.12, is solved simultaneously to correctly calculate the apparent magnitude of the desired stars.

$$m_U = (UB + BV + V) + u_1 + u_2x_U + u_3UB + u_4UBx_U , \quad (3.8)$$

$$m_B = (BV + V) + b_1 + b_2x_B + b_3BV + b_4BVx_B , \quad (3.9)$$

$$m_V = V + v_1 + v_2x_V + v_3BV + v_4BVx_V , \quad (3.10)$$

$$m_R = (V - VR) + r_1 + r_2x_R + r_3VR + r_4VRx_R , \quad (3.11)$$

$$m_I = (V - VI) + i_1 + i_2x_I + i_3VI + i_4VIx_I . \quad (3.12)$$

The instrumental magnitudes are m_U, m_B, m_V, m_R and m_I . The quantities UB, BV, VR and VI indicate the differences between measured instrumental magnitudes: $VI = V - I$. The air mass for an image taken with filter Z is given by x_Z in the transformation equations. For more on atmospheric extinction, the calibration of stellar magnitudes and a discussion on the terms of higher order extinction, see Chromey (2010).

The 25 standard stars that were used for the calibration of atmospheric extinction are given in Table 3.4. These standard stars were observed throughout the week so that the best averaged atmospheric extinction coefficients could be calculated for the images.

To calibrate extinction coefficients, an instrumental magnitude must be obtained for each standard star. The first step was to identify the centre of the star on the image and save its pixel coordinates in a text file. The background of the image becomes filled with diffused photons which originate from numerous possible sources and are assumed to be homogeneous across the image. If the light from the source is measured then background photons are included and the measurement of the light from the source is contaminated. To get a measurement for the average background over an entire image, the

Star	V	B-V	U-B	V-R	V-I
E323	9.650	0.454	0.013	0.264	0.530
E312	9.664	0.151	0.099	0.094	0.201
E575	9.324	0.886	0.583	0.481	0.907
E505	8.685	0.337	0.219	0.190	0.388
E699	8.707	0.936	0.727	0.519	0.966
E308	8.511	0.098	-0.024	0.116	0.288
E432	8.797	0.910	0.510	0.482	0.950
E4104	9.722	1.306	1.303	0.684	1.304
E532	9.237	1.510	1.890	0.811	1.557
E406	8.348	0.090	0.080	0.031	0.067
E505	8.685	0.337	0.219	0.190	0.388
E424	8.505	0.489	-0.017	0.282	0.568
E416	8.588	0.152	0.114	0.074	0.158
E607	8.780	0.119	0.104	0.072	0.154
E6100	8.218	1.060	0.791	0.515	0.987
E318	8.578	0.285	0.060	0.167	0.345
E535	8.623	1.430	1.567	0.771	1.482
E582	8.410	0.686	0.195	0.376	0.734
E623	8.996	0.534	0.062	0.311	0.614
E327	8.330	0.644	0.194	0.348	0.676
E324	8.847	0.560	0.022	0.315	0.622
E4105	8.894	1.261	1.400	0.629	1.177
E461	8.859	0.214	0.163	0.110	0.225
E569	8.896	0.920	0.527	0.498	0.974
E667	8.664	0.450	0.022	0.264	0.532

Table 3.4: The apparent magnitudes for the 25 standard stars and their intrinsic colours used to calculate the extinction coefficients to compensate for atmospheric extinction.

image was opened with `fitsview` and saved as a Table in a text file. An `Octave` program was used to calculate the most prominent pixel value across the image. The code which was used for the calculation of the average background value per pixel on the image is given in Appendix B. This was accomplished because the IRAF task needed an estimation value for the average background level. The task which was used for the calculation of the star's magnitude is `noao.digiphot.daophot.phot`. This was done by choosing an appropriate aperture for each standard star. The `phot` task used two annuli: the first including all of the light of the star, and the second to calculate the average background value in close proximity to the star. The sky annulus had an inner and outer limit, and the measurements for the background were taken in the area between the inner and outer limits of the annulus. The placement of the star and sky annulus' centres are on the maximum value of the star's profile. An estimated value for the location of star's centre was given to the task in the form of a text file containing the pixel value. The maximum pixel value of the star was then determined with a box algorithm from the surrounding area of the estimated centre.

In the calculation of the magnitude by `phot`, the background pixel value was subtracted from the

measured pixel value. The instrumental magnitude was calculated with

$$m = -2.5 \log_{10}(N) , \quad (3.13)$$

where N was the total count rate. A star observed under perfect circumstances will have a Gaussian light distribution. Using the central pixel and the FWHM of the light profile of the standard star, an equivalent normal distribution is modelled by the software. The count rate was calculated by taking an approximate pixel value for each pixel from the model and multiplying it with the weight of that specific pixel's position. The model's normal distribution spans the width of the annulus. All of the weighted values are added together and divided by the total exposure time.

After the instrumental magnitude for each standard star was determined, the extinction coefficients for equation 3.8-3.12 can be determined. With the correct extinction coefficients, the instrumental magnitude of an object can be transformed to its apparent magnitude.

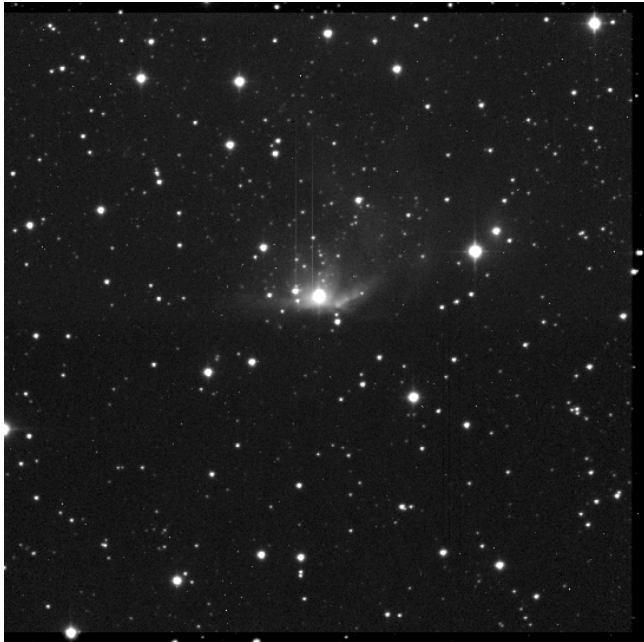
3.3.5 Point-spread-function photometry

Due to the crowded field in some parts of the image of RCW 34 it was impractical to perform aperture photometry. Instead it was necessary to do crowded field photometry, which uses software to detect and distinguish all of the light sources on the image. The brightest and most distinguishable stars on the image are selected first. Then a Gaussian profile is fitted, based on all of the selected stars, so that a representative point-spread-function is constructed that fits onto all of the detected stars.

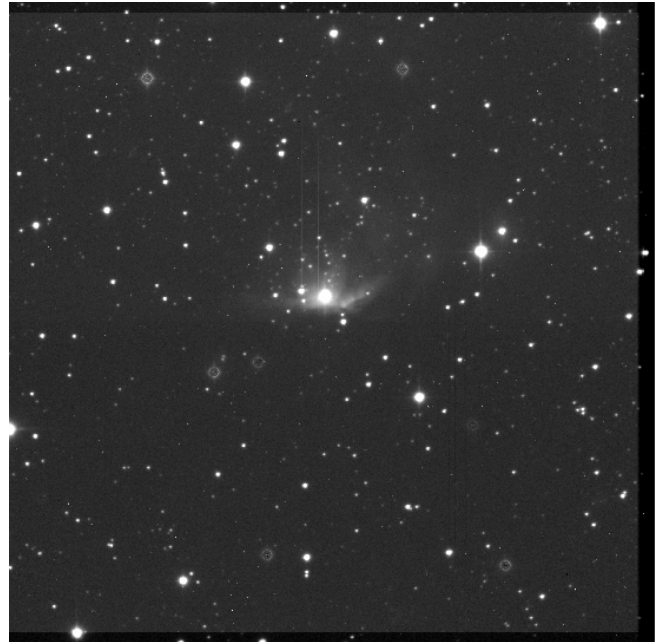
To detect all of the stars on an image such as Fig 3.4a the `noao.digiphot.daophot.daofind` task is used. The `daofind` task marks each star's pixel coordinates and the FWHM of the light distribution of the source. This is done in the same manner in which the profile of the standard star was identified, using the average background value and looking for the maximum value of each profile.

After a point-spread-function was constructed it was tested on the candidate image by subtracting the selected stars from the candidate image. If the point-spread-function was sufficient for the sources used in its construction, the subtracted image would show a region uniform with the background where the selected sources were. If the point-spread-function was not sufficient, a larger number of stars or different stars were selected for the construction of a new point-spread-function. A badly fitting point-spread-function is shown in Fig 3.4b. In the case of a good point-spread-function, the chosen point-spread-function would be applied to all of the detected light sources so that if a subtracted image was constructed, the resulting image would be clear, as shown in Fig 3.4c.

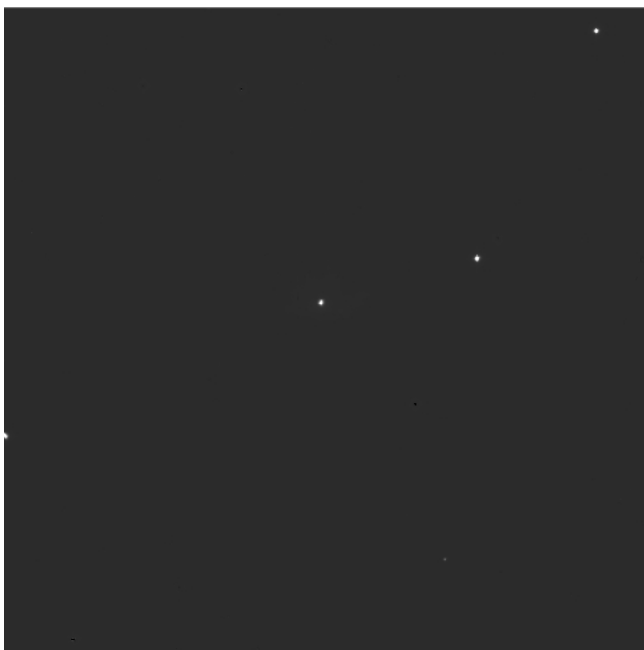
After all of the light from the stars on each image was measured with a point-spread-function, the instrumental magnitude for each star was calculated. The apparent magnitudes of the stars were calculated using the same extinction transformations used to calculate the extinction coefficients.



(a) The image after stacking and reduction.



(b) The blurred dots on the image were the stars selected for the point-spread-function.



(c) A better fitting point-spread-function was constructed from different stars and all of the light sources on the image were removed.

Figure 3.4: The I image on which crowded field photometry had to be conducted with a point-spread-function.

3.3.6 Matching source in V , R , I and R , I sets and correspondence with NIR sources

To compile a multi-wavelength set of magnitudes required a correspondence between the NIR sources that were identified by de Villiers (2009) and those obtained from this optical photometric study. To match up the sources from the two studies, the right ascension and declination for each source had to be known. As was not available for the optical sources, a transformation between pixel coordinates to ICRS (**I**nternational **C**elestial **R**eference **S**ystem) coordinates had to be made.

The transformations were constructed by selecting the stars from which the point-spread-function were constructed and marking their coordinates in a file with the name `astro.X.coo`, where X is the name of the selected filter. Next the ICRS coordinates of the chosen stars were read from a DSS (**d**igitised **s**ky **s**urvey) image of RCW 34 and were entered into a text file `astroref.coo.X`, where X is the chosen filter. A transformation between the pixel coordinates and ICRS coordinates was constructed with the `images.imcoords.cmap` task. The `cmap` task fits the distribution of points from the one set of coordinates to the other and then constructs a transformation for the remainder of the image. The fits that were used for the transformations on the x- and y-axis were of second order and χ^2 and η^2 statistical tests applied as criteria. These statistical tests are used to validate the fitting of measured quantities to those of a theoretical model, so the coordinates of the selected stars were tested against the model for the transformation from the pixel to ICRS coordinate system. The tests were successful for all of the chosen points. The transformation scales were added to the headers of the images from the individual filters with the `wcsctrans` task so that the ICRS coordinates could be calculated for any chosen point on an image. The `wcsctrans` task was used to convert the pixel coordinates for light sources that matched up on desired images to ICRS coordinates, and their coordinates and apparent magnitudes were written to new data files.

The alignment between the optical and NIR sources was accomplished with a `c++` program, given in Appendix C. The given sample of code finds matches for sources in the R and I filter with NIR sources. The coordinates for a source that matched up in the R and I were taken and then the nearest source in the NIR was sought, allowing a tolerance in the matching of $0.001''$.

A total of 481 sources were detected in all of the optical filters. However, this did not equal the number of sources that matched up in the images. The atmospheric extinction in the U and B filters is very high, so it was suspected that the most likely sources were to be found in the V , R and I filters. A total of 214 sources matched up in the R and I filters. The set of extinction equations 3.8-3.12 used for the calculation of extinction coefficients cannot be used in the solution of the apparent magnitudes of the 214 sources. This is because the transformation equations are linearly dependant on colours other than $R - I$.

A new set of transformation equations were set up so that only the R and I magnitudes were

required to calculate the apparent magnitude. The following set of transformation equations was used

$$m_R = R + r_1 + r_2 x_R , \quad (3.14)$$

$$m_I = I + i_1 + i_2 x_I + i_3 (R - I) + i_4 (R - I) x_I . \quad (3.15)$$

The standard stars observed on the same nights as the R and I images were used to calculate a new set of extinction coefficients. A list of these stars is given in Table 3.5a. Equations 3.14 and 3.15 are the linear transformations that were used to calculate the extinction coefficients shown in Table 3.6a.

Star	R	I	Star	V	V-R	R-I
E323	9.39	9.12	E323	9.650	0.264	0.530
E312	9.57	9.46	E312	9.664	0.094	0.201
E575	8.84	8.42	E575	9.324	0.481	0.907
E505	8.5	8.3	E505	8.685	0.190	0.388
E699	8.19	7.74	E699	8.707	0.519	0.966
E308	8.4	8.22	E308	8.511	0.116	0.288
E432	8.32	7.85	E432	8.797	0.482	0.950
E4104	9.04	8.42	E4104	9.722	0.684	1.304
E532	8.43	7.68	E532	9.237	0.811	1.557
E406	8.32	8.28	E406	8.348	0.031	0.067
E505	8.5	8.3	E505	8.685	0.190	0.388
E424	8.22	7.94	E424	8.505	0.282	0.568
E416	8.51	8.43	E416	8.588	0.074	0.158
			E607	8.780	0.072	0.154
			E6100	8.218	0.515	0.987
			E318	8.578	0.167	0.345
			E535	8.623	0.771	1.482
			E582	8.410	0.376	0.734
			E623	8.996	0.311	0.614
			E327	8.330	0.348	0.676
			E324	8.847	0.315	0.622
			E4105	8.894	0.629	1.177
			E461	8.859	0.110	0.225
			E569	8.896	0.498	0.974
			E667	8.664	0.264	0.532

(a) Standard stars used to calculate the extinction coefficients for equation 3.14 and 3.15.

(b) Standard stars used to calculate the extinction coefficients for equations 3.16-3.18.

Table 3.5: Standard stars used for atmospheric calibration.

The same was done for sources that matched in the V, R and I filters. By using three filters instead of just two, a colour-colour diagram could be constructed and the effects of interstellar reddening could be calculated. The set of transformations that were used to calculate the extinction coefficients and

Parameter	Value	Parameter	Value
r_1	3.66 ± 0.16	v_1	3.54 ± 0.01
r_2	-0.11 ± 0.14	v_2	0.15 ± 0.00
i_1	4.67 ± 0.12	r_1	3.41 ± 0.01
i_2	-0.01 ± 0.11	r_2	0.10 ± 0.00
		r_3	0.18 ± 0.02
		r_4	0.00 ± 0.00
		i_1	4.58 ± 0.11
		i_2	0.07 ± 0.00
		i_3	0.03 ± 0.02
		i_4	0.00 ± 0.00

(a) The extinction coefficients as calculated for the transformation equation 3.14 and 3.15.

(b) The extinction coefficients as calculated for the transformation equations 3.16 - 3.18.

Table 3.6: Coefficients for atmospheric extinction.

transform from the instrumental magnitudes to apparent magnitudes are:

$$m_V = V + v_1 + v_2 x_V, \quad (3.16)$$

$$m_R = R + r_1 + r_2 x_R + r_3 (V - R) + r_4 (V - R) x_R, \quad (3.17)$$

$$m_I = I + i_1 + i_2 * x_I + i_3 (V - I) + i_4 (V - I) x_I. \quad (3.18)$$

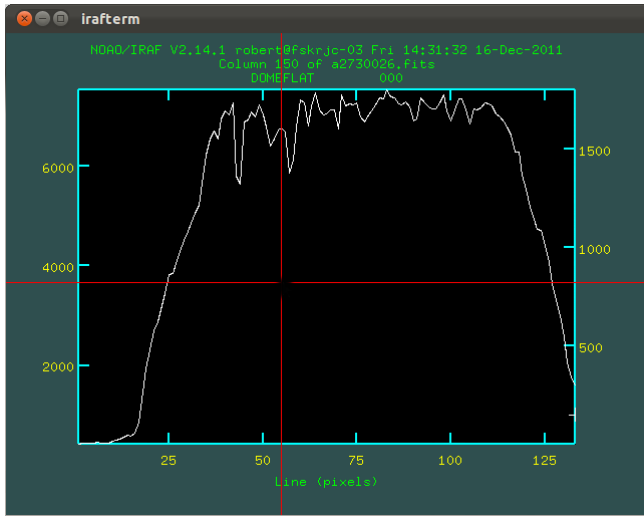
The standard stars that were used to calculate the extinction coefficients for the sources that matched in the V, R and I filters are given in Table 3.5b. From equation 3.16-3.18 and the standard stars in Table 3.5b the extinction coefficients were calculated and are given in Table 3.6b.

3.4 Spectroscopic reduction

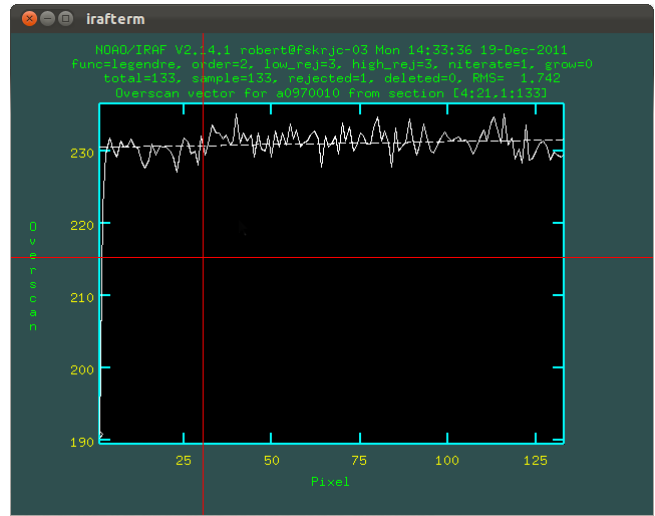
3.4.1 Manual reduction

The steps outlined in this section are similar to those found in the instruction manual for the reduction of long slit spectra as found on the website of the IRAF software suite (<http://iraf.net/irafdocs/spect/>).

The images for both the 2002 and 2011 data sets have the dimensions of 1798×133 pixels, representing the entire CCD before reduction. The software package used in IRAF for the reduction of the long slit spectra was `noao.imred.spectred`. The images for 2002 and 2011 had the values for the BIAS and trim sections inserted as image headers. These values were not satisfactory, due to the distribution of light on the CCD. The first step was to determine new values for the OVERSCAN regions and where the images were to be trimmed. Next, the areas close to the edge of each image were inspected so that any variations on the image or CCD could be corrected with the overscan routine. A dome flat was used for this inspection, as shown in Fig 3.5a.

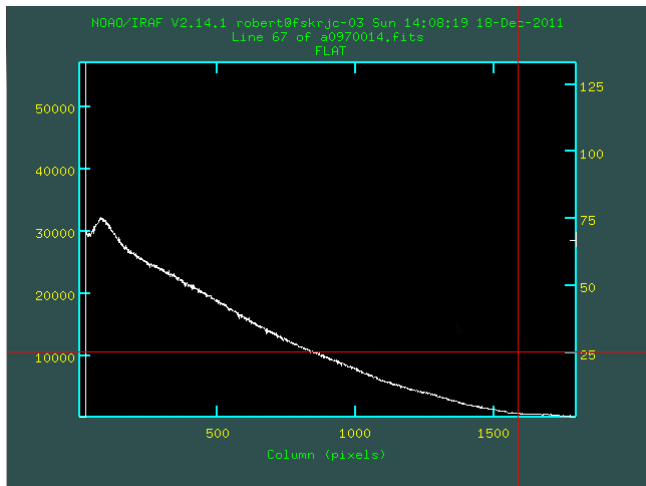


(a) A lineplot across a column for a raw image of a dome flat. There is no clear dispersion line visible, due to the image being out of focus. The OVERSCAN was used to determine any variation across the width of the CCD image. A linear Laplace polynomial was fitted through the regions where the signal is strong enough. The signal from column 1-24 was too low to do a significant OVERSCAN fit, but columns 25-133 had a strong enough signal.

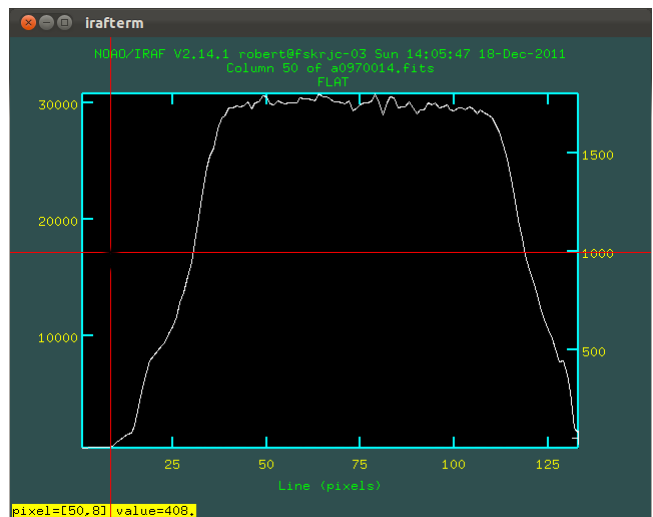


(b) The region selected for the OVERSCAN fitting is shown above. A second order Lagrange function was used to fit the OVERSCAN in all of the images.

Figure 3.5: Aids to selecting the OVERSCAN regions of the spectral images of 2002.



(a) The uniform distribution of the dome flat is used to correct any variations across the length of the CCD chip.



(b) The usable region of the image extends from where the signal has a significant strength. For the case of the images taken in 2002, it is from pixel value 24 and upwards in width.

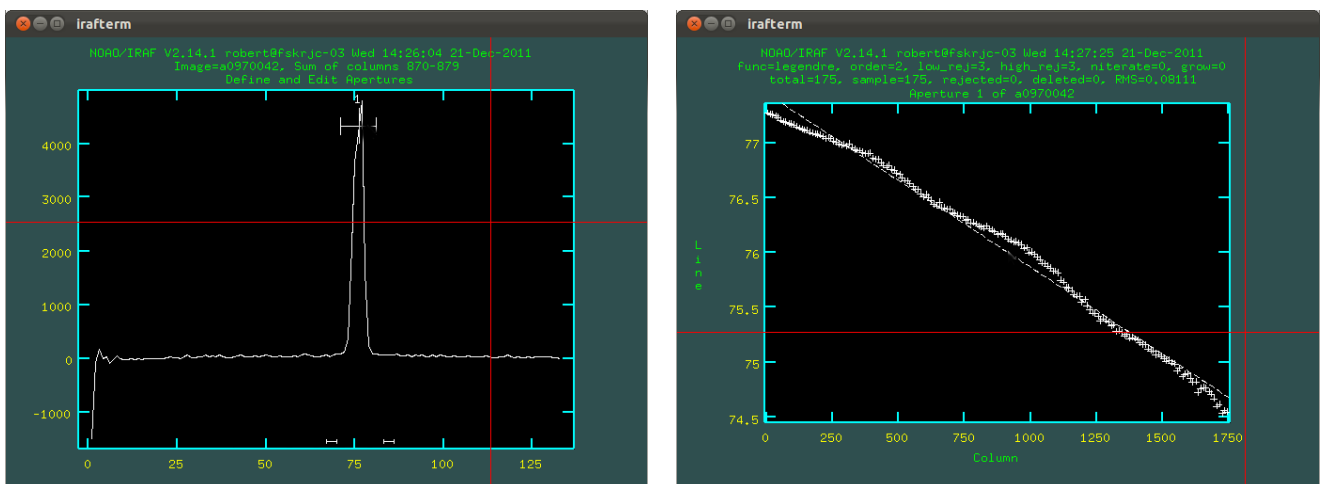
Figure 3.6: Light distribution of dome flat image and usable regions of the spectral images.

The OVERSCAN region for the images that were used in the set of 2002 is [24:1772,1:133], as shown in Fig 3.6b. The region used for the set of 2011 was [4:21,1:133]. The variations in the OVERSCAN region across the chip were used to calculate the variations in the BIAS data across the chip. This

variation was fitted with a second-order Lagrange function.

As with the reduction of the photometric images, a BIAS image was constructed to account for read-out noise for the data sets of 2002 and 2011. For the data observed in 2002, a set of 10 BIAS images were combined with a median routine in the `imcombine` package. The data set for 2011 had a set of 20 BIAS images that were stacked in the same manner.

After the BIAS image was constructed, it was used to subtract the read-out noise from the images of the spectral lines, arcs and `flatfield` images with the `noao.imred.ccdred.ccdproc` package. In the same instance the OVERSCAN regions were used to subtract the effects of thermal electrons. The the edges containing the OVERSCAN regions were then trimmed away.



(a) The position of the aperture line as chosen along the width of the CCD

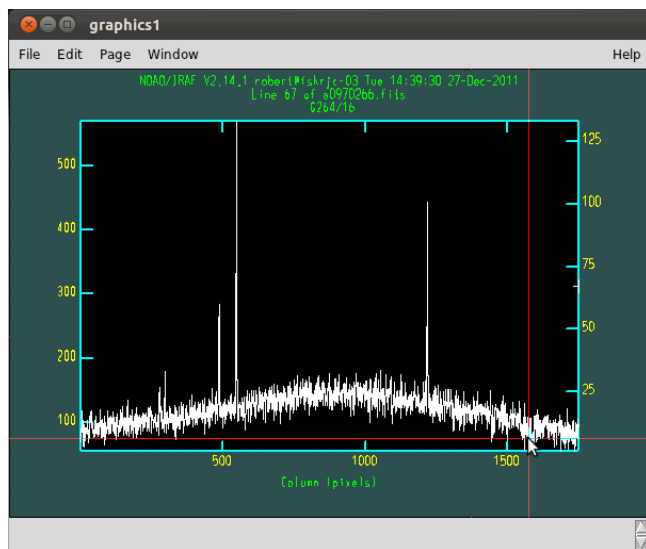
(b) The aperture line along the CCD chip and the profile of the line which will be used to extract the spectral profile from the image

Figure 3.7: Aids to fitting the aperture and extracted profile from the aperture.

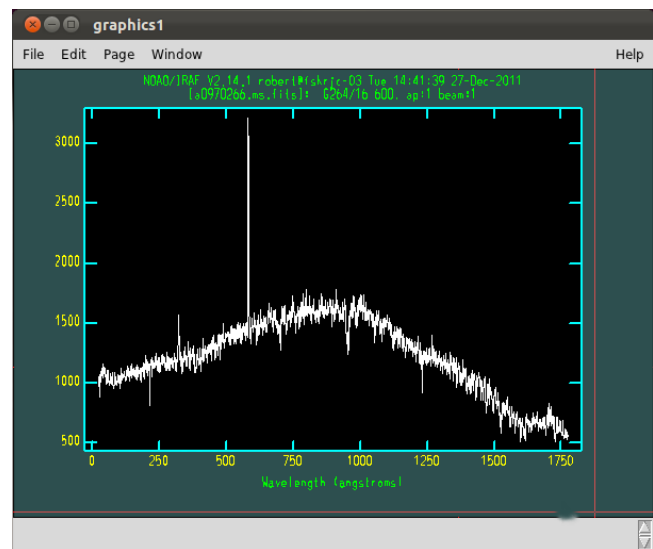
After this process, the images could be used for scientific measurements. The aperture line of the spectral profile had to be characterised next. The aperture of the stellar light is not always perfectly aligned with the CCD, so the light of the stellar spectral profile may run across a few of the rows on the CCD. To see if this has occurred, a few slices of rows over the image are plotted and inspected for aperture peaks at the same columns. The task used to mark the aperture line on the CCD was `noao.imred.specred.apfit`. In the images of 2002 and 2011 the direction of the dispersion axis across the CCD had to be declared, being along the y-axis instead of the default x-axis direction. This was done by adding a header to all of the images with the value "`DISPAXIS 1`". The aperture profile for each image varies slightly from the other images due to numerous factors. These factors could be the star going out of focus for short periods due to atmospheric conditions, the star drifting out of the slit due to the tracking of the telescope which is not perfect for long exposure periods etc. The default value for the aperture size for images taken in 2002 is 5 pixels, and 3 pixels for the images taken in 2011. A second order Legendre polynomial function was used for fitting the traced profile of

the aperture line along the CCD.

When the light from the star shines onto the grating and then reflects onto the CCD, one only has pixel coordinates for the spectral features. Therefore wavelength calibration had to be done for the transformation from the pixel coordinates to wavelength coordinates. This was achieved by shining a Cu-Ar arc lamp onto the grating and using characteristic emission lines with corresponding wavelengths to achieve a transformation from pixel coordinates to wavelength values for the arc images. Three or four emission lines are selected on the first arc image and then the other features are automatically identified with their corresponding wavelength values. A third-order spline was used to calculate a transformation from the pixel coordinates to wavelength values in Å. The first arc image's transformation is then used as a template for the other arc images. Each arc image is checked when assigning wavelength values to the emission line profiles from the first image's template. There are usually two arc images for each image of a spectral profile from a star. The coordinates of the aperture marking the emission profile of the star were used on the arc images to calculate transformations from pixel coordinates to wavelength values. The transformation for each of the two arcs is used to construct an average transformation for the spectral profile of the star. The task `noao.imred.spectred.apall` was used to do the wavelength calibration on the images taken from the arc lamp. A standard profile for the wavelength profile of the arc lamp was provided so that three or more emission lines could be selected with their corresponding wavelengths.



(a) A cross sectional plot of a column which lies in the region of the CCD that was used in the spectral extraction of the spectral profile



(b) The spectral profile as extracted by the `apall` package from the image from which the sectional profile is displayed in Fig 3.8a

Figure 3.8: Cross section of reduced spectral image and extracted spectral profile.

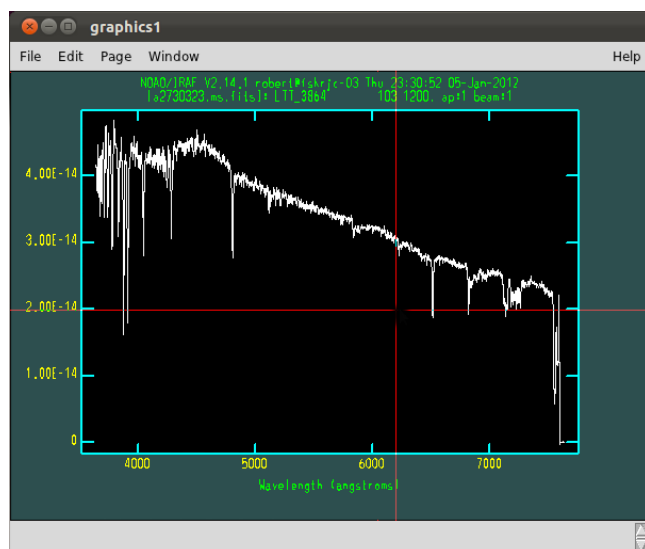
A list of all of the arc images was compiled so that the first in the sequence was used as a template for the rest of the arc images because the other arc images would differ very slightly from the first image. The `apall` package extracted all of the apertures from the arc images according to those that

were marked on the images of the stellar spectra. The wavelength calibration for a spectral profile was done by using the average transformation between two arc lamp images that were taken before and after a spectral image was taken. The `apall` package sorted and processed the spectral and arc images according to their Julian dates. The arc images that were used for the 2002 observations did not have a template from which the wavelength values could be read. To do the wavelength calibrations for the observations that were taken in 2002, standard star profiles were used by marking the wavelength values for the $H\alpha$, $H\beta$ and $H\gamma$ absorption lines. A linear transformation could be constructed from the three points that were marked for the wavelength calibration. The same standard star image was used in the calibration of the wavelength for all of the images in the 2002 data set. The calibration with the standard star's profile was and precise enough to identify emission/absorption lines other than those used for the calibration.

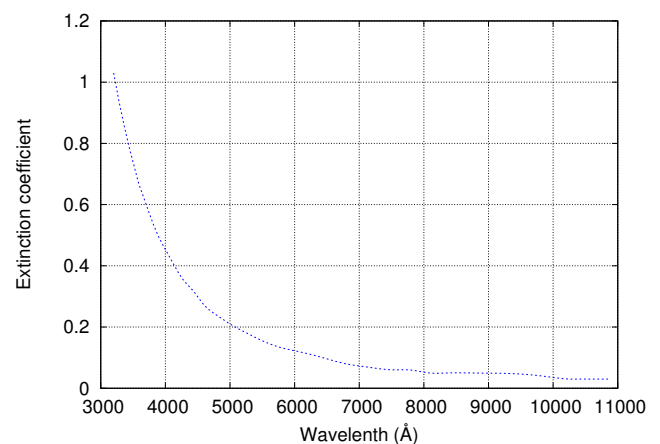
The `apall` package extracted the spectral profiles and also calculated the extinction from the air mass header that was given in each `FITS` image, using the extinction profile shown in Fig 3.9b.

3.4.2 Automatic reduction

The data set of the 2011 observations was reduced with the `noao.imred.specred.doslit` package, which contain all of the steps that were performed in the manual reduction in a collected set of procedures. All of the parameters used in the `doslit` package had to be given in the configuration list before the package could be run.



(a) The standard star LTT 3864 used for normalisation and flux calibration of the spectral profiles in the 2011 data set.



(b) The extinction as a function of wavelength for the long slit spectrograph on the 74'' telescope in Sutherland. Data obtained from the SAAO's website.

Figure 3.9: The standard star that was used for calibration and the average atmospheric extinction for Sutherland.

A standard star was used to normalize the extracted spectral profile of each star in the data set of

2011 and do flux calibration. This standard star was chosen from the list of suggested standard stars in the manual of the long slit spectrograph for the 74" telescope. IRAF has a flux profile for LTT-3864 in the CTIO (CERRO TOLOLO INTER-AMERICAN OBSERVATORY) library of one dimensional spectral profiles. The flux profile, coordinates and broadband spectrum can be found on page 103 in Worters (2010). This makes it possible for IRAF to calculate the flux of the other spectral profiles in the data set. An observation of the standard star was conducted on each night of the week so that a good average flux calibration could be calculated. The star chosen was LTT-3864, which is a standard white dwarf, and the reason it was chosen is that from all the stars in the list, it was the closest to RCW 34. The spectral profile of the standard star is given in Fig 3.9a.

The flux calibration was the final step in the reduction of the 2011 spectroscopic set. Using the extracted spectra it was possible to do analysis and identify which absorption and emission lines are present in the spectral profile of the star. In the following chapter the results from the photometric and spectroscopic observations will be presented and discussed.